Fluorine-free and hydrophobic hexadecyltrimethoxysilane-TiO2 coated mesh for gravity-driven oil/water separation

Cai, Yongwei; Zhao, Qi; Quan, Xuejun; Feng, Wei; Wang, Qingkuo

Published in:
Colloids and Surfaces A: Physicochemical and Engineering Aspects

DOI:
10.1016/j.colsurfa.2019.124189

Publication date:
2020

Document Version
Peer reviewed version

Author Accepted Manuscript version of Cai, Yongwei et al. "Fluorine-free and hydrophobic hexadecyltrimethoxysilane-TiO_2 coated mesh for gravity-driven oil/water separation". *Colloids and Surfaces A: Physicochemical and Engineering Aspects*. 2019. https://doi.org/10.1016/j.colsurfa.2019.124189

Fluorine-free and hydrophobic hexadecyltrimethoxysilane-TiO_2 coated mesh for gravity-driven oil/water separation

Yongwei Cai [a, b] *, Qi Zhao [b] *, Xuejun Quan [a], Wei Feng [a], Qingkuo Wang [a]

[a] *Department of Chemistry and Chemical Engineering, Chongqing University of Technology, Chongqing, 400054, PR China*

[b] *Department of Mechanical Engineering, University of Dundee, Dundee DD1 4HN, UK*

ABSTRACT: Superhydrophobic and superoleophilic meshes have attracted great attention in oil/water separating application. However, superhydrophobic surfaces are not only complicated in preparation but also easy to break in practical applications. In this paper, we prepared fluorine-free hydrophobic hexadecyltrimethoxysilane (HDTMS)-TiO_2 coated meshes with properties of cost-effectiveness, easy to manufacture, and high separation efficiency by a liquid phase deposition method. The surface topography, composition, and functional groups of the meshes were characterized by field emission scanning electron microscope (FE-SEM), energy dispersive X-ray spectroscopy (EDS), X-ray photoelectron spectroscopy (XPS), and Fourier transform microscopic infrared spectrometer (FT-IR) spectrum, respectively. A new gravity-driven oil/water separator was designed for the separation experiments. The separation efficiency of the hydrophobic HDTMS-TiO_2 coated meshes maintained over 97.8% after 35 separating cycles. This study indicated that the superhydrophobicity of the separating mesh was nonessential for the highly efficient oil-water separation. The fluorine-free hydrophobic HDTMS-TiO_2 coated meshes provided an economical and beneficial solution to treat

industrial oily wastewater mixtures and environmental oil spills.

Keywords: Oil/water separation, Hydrophobic coating, TiO_2, HDTMS, Fluorine-free

1. Introduction

Oil/water separation has become a crucial and urgent issue due to the large amount of industrial oily wastewater and increasingly frequent oil spill accidents. [1, 2] The discharge of oily wastewater not only results in the waste of petroleum resources, but also is responsible for serious pollution to water sources and soil, as well as leading to the death of living organisms because of the lack of oxygen in the water. [3, 4] Therefore, how to effectively treat oily waste water, to achieve water reuse and oil recovery, and to protect the environment have received increasing attention from the state and the society.[5, 6] Traditional technologies, such as gravity separation[7], skimming[8], sorption[9, 10], and flotation[11] are beneficial for the separation of oil/water mixtures but they afflict with low efficiency and high operation cost.

Many attempts have been made to coat the meshes with superwettability [12] for highly efficient oil/water separation. [13-19] Feng et al. [20] for the first time proposed a superhydrophobic/superoleophilic tetrafluoroethylene (PTFE)/stainless steel mesh in oil/water separation. The water static contact angle of the superhydrophobic coating was 156.2°, the rolling angle was 4°, and the contact angle of diesel oil was close to 0°. The prepared mesh allowed rapid passage of the oil phase while the water phase was completely blocked. Yang et al. [21] prepared a superhydrophobic copper mesh by one-step immersion method in stearic acid/ethanol solution. The as-fabricated mesh demonstrated a separation efficiency of larger than 97% for different oil/water mixtures. Zhang et al.[13] prepared the superhydrophobic and superoleophilic copper wire mesh via one-step anodization process in myristic acid/ethanol solution for water-oil separation. The separation efficiency of the mesh could reach above 87% after 10 cycles. Xu et al. [22] fabricated superhydrophobic nano-Al films on stainless steel meshes via electrophoretic deposition process. The separation efficiency for continuous oil/water separation was up to 95.8 ± 0.9%. Wang et al. [17] fabricated a fluorine-free superhydrophobic steel mesh by depositing with micro/nano Polystyrene@SiO_2@HDTMS

(Hexadecyltrimethoxysilane) particles. The as-prepared mesh showed efficient and rapid oil/water separation. Dong et al. [23] prepared a TiO_2 coated stainless steel mesh with underwater superoleophobicity and corrosion resistance via sol-gel method. The separation efficiency of the meshes for all oils was above 99.5% and remained high separation efficiency even after 40 cycles. However, many superhydrophobic surfaces are susceptible to damage because of the fragile micro/nano-structures on them.[24-27] On the other hand, maintaining highly efficient and stable performances for superhydrophobic materials for a long time still remains a challenge so far[28] which greatly restricts the large-scale application of the superhydrophobic meshes in the field of oil-water separation. Compared with superhydrophobic material surfaces (water contact angles higher than 150° and water sliding angle less than 10°), hydrophobic surfaces (water contact angles higher than 90°) are more common in nature and could be fabricated more easily and economically for practical use [29]. Consequently, it is worthy to explore whether the normal hydrophobic coated meshes have the same performance as the superhydrophobic meshes in oil/water separation.

Hydrophobic agents, fluoroalkylsilanes (FAS), [14, 30, 31] are usually used to modify coatings to obtain hydrophobic or superhydrophobic surfaces, because these fluorochemicals have extremely low surface free energy. [32] However, these compounds are expensive and environmentally unfriendly, which could discharge highly toxic substance such as perfluoroalkyl carboxylates, or perfluoroalkyl sulfonates into environment.[33, 34] Therefore, many attempts have been made to develop the coatings modified with non-fluorinated chemicals.[17, 35-37] Fluorine-free HDTMS is a beneficial candidate to form hydrophobic and superhydrophobic surfaces.[38] However, direct coating of HDTMS on the metal surfaces is nondurable and does not effectively reduce the surface energy because the silane of alkoxysilanes on the steel substrate is weak due to the sensitivity of Fe-O-Si bond to hydrolysis[39]. Accordingly, the ceramic material coatings, such as TiO_2 [40, 41], Al_2O_3 [42, 43], SiO_2[44, 45], ZnO[4, 46], ZrO_2 [47], and MFI-type zeolite[48] are widely applied to bridge the functional groups and the substrates, and successfully applied in the separation processes of the oil/water mixtures. As a ceramic

material, TiO_2 has high impedance and nontoxic properties [49] and has a beneficial potential for the oil/water separation area [50].

In this paper, we prepared a TiO_2 coating on the AISI type 304 stainless steel meshes with a liquid phase deposition method [40, 51], and then modified the coating with the fluorine-free HDTMS chemical to obtain the hydrophobic HDTMS-TiO_2 coated meshes. The surface topography, the composition, and the functional groups of the meshes were characterized as well as the static contact angles (SCA) of the coated meshes were investigated to explore the hydrophobicity of the meshes. Moreover, the oil/water separation experiments were carried out using a home-made oil/water separator with the hydrophobic HDTMS-TiO_2 coated meshes. Furthermore, the separation properties of the as-prepared meshes were evaluated for the oil/water mixtures.

2. Experimental

2.1. Materials

Hexadecyltrimethoxysilane (HDTMS, $H_3C(CH_2)_{15}Si(OCH_3)_3$, 85%) was purchased from Aladdin. Ammonium hexafluorotitanate (IV) ($(NH_4)_2TiF_6$, 98%) was acquired from Tianjin Guangfu Fine Chemical Research Institute, China. Boric acid (H_3BO_3, 99.5%), absolute ethyl alcohol, and acetone were purchased from Chengdu Kelon Chemical Reagent Factory, China. Sodium hydroxide (NaOH) was attained from Shanghai Chemical Reagent Factory, China. Hydrochloric acid (HCl, 36.0-38.0 *wt.*%) was obtained from Chongqing Sichuan East Chemical (group) Co. LTD, China. Senior red ink (855 type) was purchased from Guizhou Doctor Chemical Co. LTD, China. Different types of oils and organic solvents were selected for oil/water separation. Fuel oil, diesel oil (No. 0), was obtained from China Petrochemical Corporation (Sinopec Group). Cooking oils, such as rapeseed oil, peanut oil, and soybean oil, were purchased from local Yonghui Supermarket of China. Organic solvent, chloroform, was acquired from East Sichuan Chemical Co., Ltd, Chongqing, China. AISI type 304 stainless-steel mesh of 400/inch used as a filter substrate was procured from Shanghai Yan Jin Filter Factory, China.

2.2. Preparation of hydrophobic HDTMS-TiO_2 coatings

The TiO_2 coatings were prepared with the liquid phase deposition method on the AISI

type 304 stainless steel (SS) meshes. The SS meshes were cleaned sequentially with 3 *wt.*% NaOH solution, acetone, and absolute ethyl alcohol at 40 °C for 15 min in a high-power numerical control ultrasonic cleaner (KQ-400KDE, Kunshan Ultrasonic Instrument Co., Ltd., China). The meshes were then rinsed with deionized (DI) water. The cleaned meshes were plunged in a container with the deposition solution of hexafluorotitanate ammonium ($(NH_4)_2TiF_6$) and boric acid (H_3BO_3) with the concentration ratio of 0.1:0.2 M in water baths (HH-4, Jiangsu Jintan Zhangda Instrument Factory, China) at 30 °C after the deposition time of 5, 10, and 20 h, separately, to prepare the TiO_2 coated meshes with different thickness. After the TiO_2 coated meshes were taken out, they were washed with DI water and dried in air. Finally, the meshes were sintered in a muffle furnace (SX2-10-12, Shanghai Aixi Electric Furnace Factory, China) programed with heat rate 2 °C/min, terminal temperature 300 °C, 400 °C, and 500 °C, separately, and holding time 2 h.

The hydrophobic regent (HDTMS) was grafted onto the TiO_2 coatings to gain the hydrophobic meshes. HDTMS can hydrolyze methoxy groups to generate silanol groups [52] and to form CH_3-$(CH_2)_{15}$-Si groups on the TiO_2 coatings, leading to the coating to be hydrophobic. Fig. 1 shows the preparation procedure of the hydrophobic HDTMS-TiO_2 coating on SS mesh. First, 3 vol% of HDTMS was added to a solution containing ethanol and DI water at 87: 10 vol% under magnetic stirring (HJ-3 thermostatic magnetic stirrer, Jiangsu Jintan Zongda Instrument Factory, China) at 30 °C. Then the HDTMS was hydrolyzed by standing for 24 h to obtain a hydrophobic modified solution [42]. The TiO_2 coated meshes were dipped into the solution statically for 1 h in a water bath at 30 °C, and then the modified coating meshes were dried at 120 °C for 2 h in a constant temperature oven (SK101 digital display drying oven, Shanghai Shengke Instrument Equipment Co., Ltd., China).

The forming mechanism of the hydrophobic coating could be elucidated as follows: in the hydrophobic modified solution, one HDTMS was hydrolyzed to one hexadecylsilanol and the -OH groups at the polar end of the hexadecylsilanol molecule were obtained. The number of the hydroxyl groups was three times of the hexadecylsilanol molecules. On the other hand, due to the hydrophilicity of TiO_2 coating, TiO_2 on the coating surface adsorbed

a large amount of -OH, which led to the chemical link between hexadecyl groups and three-dimensional Ti-O-Si network structures [53]. As a result, the long-chain alkyl-functionalized TiO_2 nanoparticles with Si-O-Ti three-dimensional network structures were obtained, as shown in Fig. 1.

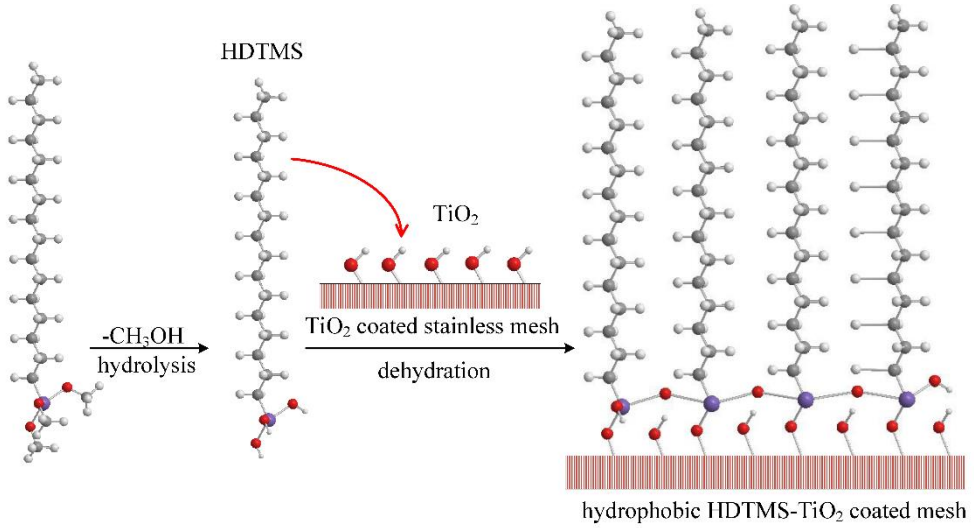

Fig. 1. Formation scheme of the hydrophobic HDTMS-TiO_2 coatings on the AISI type 304 stainless steel meshes.

2.3. Sample characterization

Surface morphologies of the meshes were characterized by Zeiss FE-SEM (Carl Zeiss, Model Neon 40 EsB CrossBeam, Germany) at a voltage of 2 kV. Chemical compositions were explored using EDS (Energy Dispersive Spectrometer). The chemical composition of the HDTMS-TiO_2 coated mesh was characterized using an X-ray photoelectron spectroscopy (XPS, Thermol Scientific Escalab 250Xi, USA) with Al radiation under the scan resolution of 0.1 eV, the scan voltage of 15 kV, and the electric current of 12.8 mA. CasaXPS software (Casa Software Ltd.; http://www.casaxps.com/) was used to process the XPS data and individual peaks were fitted to a Gaussian/Lorentzian (GL) function for each component of the element envelopes. The chemical structure of the HDTMS-TiO_2 coated mesh was also analyzed by Fourier transform microscopic infrared spectrometer (FT-IR) spectrum in the range of 550–4000 cm^{-1} using a Thermo Scientific™ Nicolet™ In™10 (ThermoFisher Scientific) with 64 scans and 1 cm^{-1} resolution. The static contact

angles (SCA) were measured with the optical contact angle/surface and interfacial tension meter (DropMeter™ A-200, MAIST Vision Inspection & Measurement Co., Ltd, China) at room temperature. A sessile drop of 2 μL of water was produced on the mesh during the SCA measurements.

2.4. Intrusion pressure and oil/water separation properties

To further investigate the separation property of the hydrophobic HDTMS-TiO_2 coated mesh, the water intrusion pressure was measured, which demonstrated the maximum height (h_{max}) of the water column that the coated mesh could support. Fig. 2a shows the schematic device for testing the intrusion pressure of the hydrophobic coated mesh. The hydrophobic mesh was horizontally placed on the flanges of the two vertical organic glass tubes with the inside diameter of 50.1 ± 0.3 mm. The mesh was sealed between two silicone gaskets, and two flanges were then tightly connected with the stainless-steel bolts to prevent leakage. DI water was injected from the upper inlet and the underneath of the hydrophobic mesh was observed. The height of the water column in the tube was recorded when the first DI water drop penetrated the mesh. The water intrusion pressure (P) was calculated with Eq. (1). [54]

$$P = \rho g h_{\max} \quad (1)$$

where, ρ is the density of water, $kg \cdot m^{-3}$; g is the gravitational acceleration, $m^{-2} \cdot s^{-1}$; and h_{max} is the maximum water column that the hydrophobic coated mesh can bear, m.

The home-made oil/water separator was designed and fabricated which consists of two pieces of organic glass tubes with inside diameter of 50.1 ± 0.3 mm. The mesh was placed on the flanges of two tubes and sealed between one pair of silicone gaskets. The flanges were fastened with four sets of stainless-steel bolts and nuts to prevent leakage, as shown in Fig. 2b. The home-made separator was fixed on two iron platforms with tube inclined 10-15° downwards along the outlet end. Fig. 3 shows the design details of the oil/water separator. All of the separator parts are made of organic glass except for the bolts and the nuts as well as the gaskets. The inner diameter of the silicone gasket is the same as that of the plexiglass tube. Therefore, the cross-section size of the mesh between

the gaskets for the oil/water separation channel is equal to the inner diameter of the plexiglass tube. The home-made intrusion pressure testing device in Fig. 2a has a similar structure with the oil/water separator.

To assess the separation quality of the hydrophobic mesh, mixtures of oil and water (50%, v/v) were prepared by mixing diesel oil, rapeseed oil, sunflower oil, and chloroform with water, respectively. The oil/water mixture was added at a constant rate from the separator inlet of Tube A. The water outlet of Tube A in Fig. 2b should be blocked with a silicone tube and a clip during the separation test to prevent the oil/water mixture flowing out of the Tube A. The clip at the water outlet would be opened intermittently to discharge the separated water phase. After the separation procedure, the oil and water were collected separately in the beakers and the volume of the two received liquids were measured. [14] Before the separation experiments, water was colored with the senior red ink to distinguish the interface between the oil and water. Due to the red ink did not dissolving in oil, oil maintains the primary color during the separation tests. The separation efficiency, η, was defined as Eq. (2):[14]

$$\eta = \frac{V_1}{V_0} \times 100\% \tag{2}$$

where, V_0 and V_1 are the volume of the oil before and after the separation process, respectively, mL.

The permeate flux was also determined by calculating the oil phase volume permeating the unit coated mesh area per unit time according to Eq. (3). [3, 21]

$$J = {(m/\rho)}\Big/{(S \times t)} \tag{3}$$

where, J is the permeate flux of the coated mesh, $mL \cdot m^{-2} \cdot s^{-1}$; m is the oil mass penetrating the coated mesh measured with a multifunctional electronic balance (AL 104, METTLER Dolly Instruments (Shanghai) Co., Ltd.) during the oil/water separating tests, g; ρ is the density of the oil, $g \cdot mL^{-1}$; S is the effective area of the coated mesh for oil passing, m^2; and t is the permeation time, s.

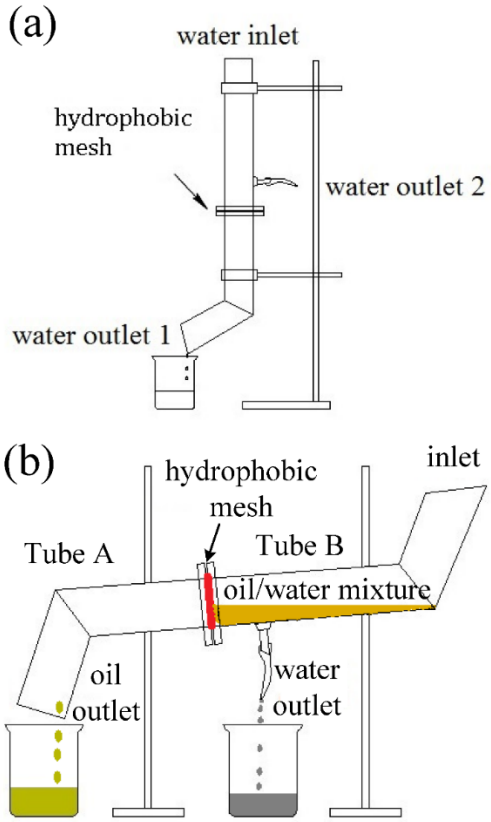

Fig. 2. Scheme diagram of the home-made intrusion pressure testing device and oil/water separator. (a) Intrusion pressure testing device; (b) oil/water separator.

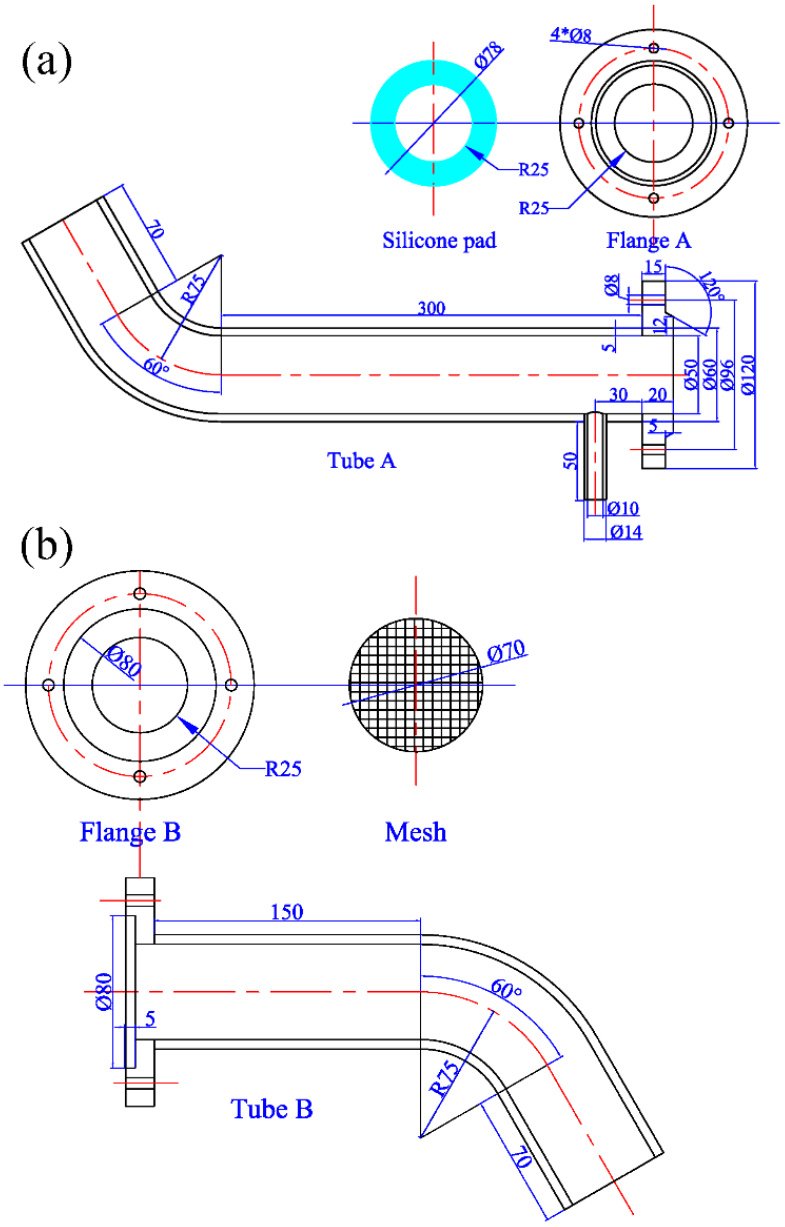

Fig. 3. Design details of the home-made oil/water separator. (a) Tube A, silicone pad and flange A; (b) tube B, flange B, and the separating mesh.

3. Results and discussion

3.1. Surface morphology and chemical characterization

The surface topography of the HDTMS-TiO_2 coated mesh with deposition time of 20 h and the sintering temperature of 400 °C as well as the uncoated SS mesh were examined by FE-SEM. Fig. 4a shows the FE-SEM image of the pristine SS mesh. The result indicated

that the SS mesh had the rectangular holes with an average side length about 80×100 μm (400 mesh sizes). Fig. 4b-e show the morphology and the structure of the TiO_2 coating on the SS mesh. The TiO_2 particles deposited on the SS surface to form the TiO_2 coating and the micro-rough surface. Fig. 4f shows the selected region of the coated mesh for the EDS analysis. Fig. 4g shows the EDS spectra. The corresponding weight and atom percentages of the selected region are given in Table 1. The results showed that the major elements in the coating were C, Fe, O, Ti, Si, Cr, and Mn. Fe, Cr, and Mn were from the SS mesh substrate. Ti and O were from the TiO_2 coating. Si and C were from the HDTMS.

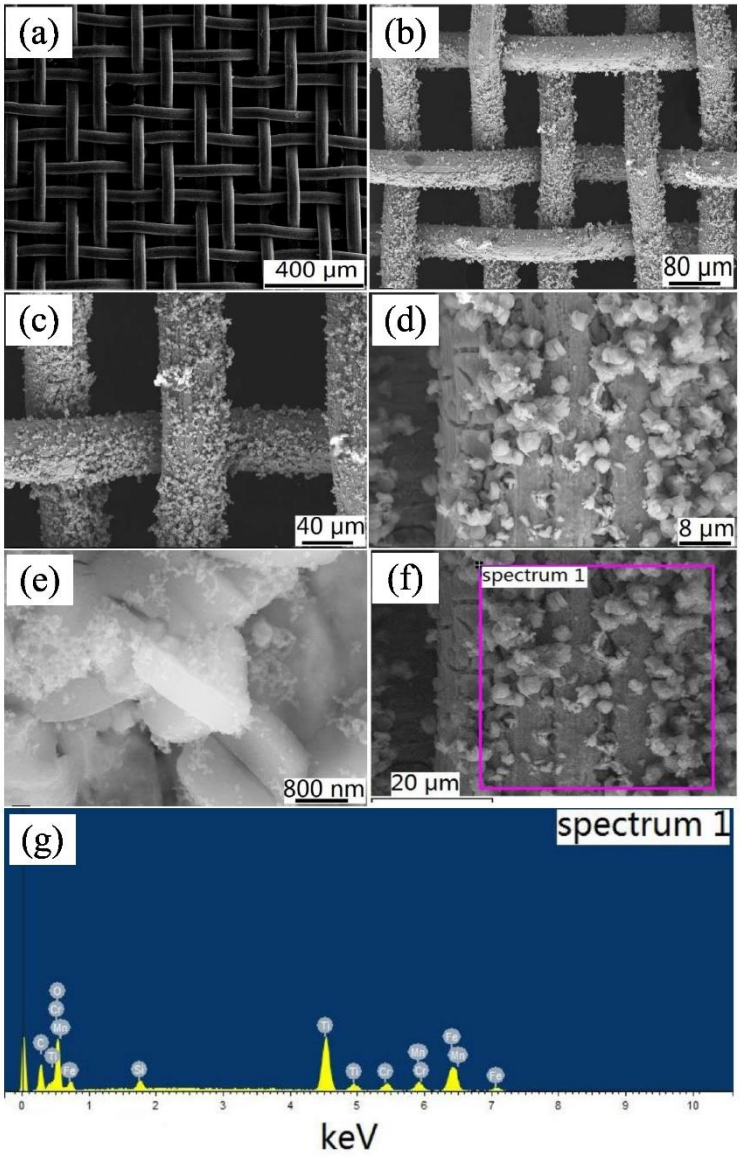

Fig. 4. FE-SEM and EDS analysis of the uncoated SS mesh and the HDTMS-TiO_2 coated mesh with the deposition time of 20 h and the sintering temperature of 400 °C. (a) FE-SEM of the

uncoated SS mesh; (b) FE-SEM of the HDTMS-TiO_2 coated mesh magnified with 500X; (c) FE-SEM of the HDTMS-TiO_2 coated mesh magnified with 1000X; (d) FE-SEM of the HDTMS-TiO_2 coated mesh magnified with 5000X; (e) FE-SEM of the TiO_2 particles on the mesh magnified with 50000X; (f) Selected region on the HDTMS-TiO_2 coated mesh for EDS analysis; (g) EDS spectrum of the selected region from (f).

Table 1. Element components of the HDTMS-TiO_2 coated mesh by EDS.

Element	*wt.*%	*at.* %	Element	*wt.*%	*at.* %
C	13.55	29.15	Cr	4.67	2.32
O	24.60	39.73	Mn	6.65	3.13
Si	1.26	1.16	Fe	26.85	12.42
Ti	22.42	12.09	Total	100.00	100.00

X-ray photoelectron spectroscopy (XPS) spectra were employed to further prove the composition of the hydrophobic HDTMS-TiO_2 coated mesh with the sintering temperature of 400 °C and the deposition time of 20 h. Fig. 5a shows the full scan survey spectra of the hydrophobic mesh. The binding energies of 710.1 eV, 532.9 eV, 284.5 eV, and 102.2 eV in Fig. 5a corresponded to the peaks of Fe2p, O1s, C1s, and Si2p [55], respectively. The strong peak of C1s indicated the presence of C-H and C-C bonds from the HDTMS hydrocarbon chain. Two characteristic peaks with binding energies of 153.1 eV (Si 2s) and 103.1 eV (Si 2p) also forcefully confirmed the presence of HDTMS chains in the coating. High-resolution narrow scans were performed on the distinct peak regions to evaluate the components of the hydrophobic HDTMS-TiO_2 coating, as shown in Fig. 5b-d. The background for each peak was selected to calculate the peak area. The results indicated that the atomic concentration of the elements of C, O, and Si in the HDTMS-TiO_2 coating was 73.9%, 16.8%, and 5.1%, respectively. It should be noted that other weak peaks were not listed in the calculating results. The XPS spectra of C1s were resolved into four Gaussian components after subtracting the background by using the fitting method. The first peak located at the binding energy of 284.3 eV was due to C-C group. The second peak

at 284.9 eV corresponded to the C-Si group [56]. The third peak at 286.4 eV attributed to the C-O group (Fig. 5b).[55] The fourth small peak at 287.7 eV was due to the C=O group [55]. The area contribution ratio of these four peaks was about 66.1: 16.4: 11.8: 5.7. Fig. 5c shows the high revaluation of the Si2p spectra which consisted of a doublet of $Si2p_{3/2}$ and $Si2p_{1/2}$ peaks with two symmetric peaks situated at 102.9 eV and 102.2 eV, respectively. [55] The area ratio of these two peaks was 5.2. Fig. 5d shows the O1s spectra, and this spectrum could be resolved into three components. The peaks located at 529.9 eV, 532.1 eV, and 534.3 eV corresponded to the groups of Si-O, -OH, and free H_2O, respectively.[55] The area ratio of these three peaks was 5.9:1.1:1. The peaks of C-Auger and O-Auger attribute to the X-ray excited auger electron spectroscopy (AES) spectra, which were the unavoidable satellite peaks of the XPS. However, AES peaks were not analyzed in this work.

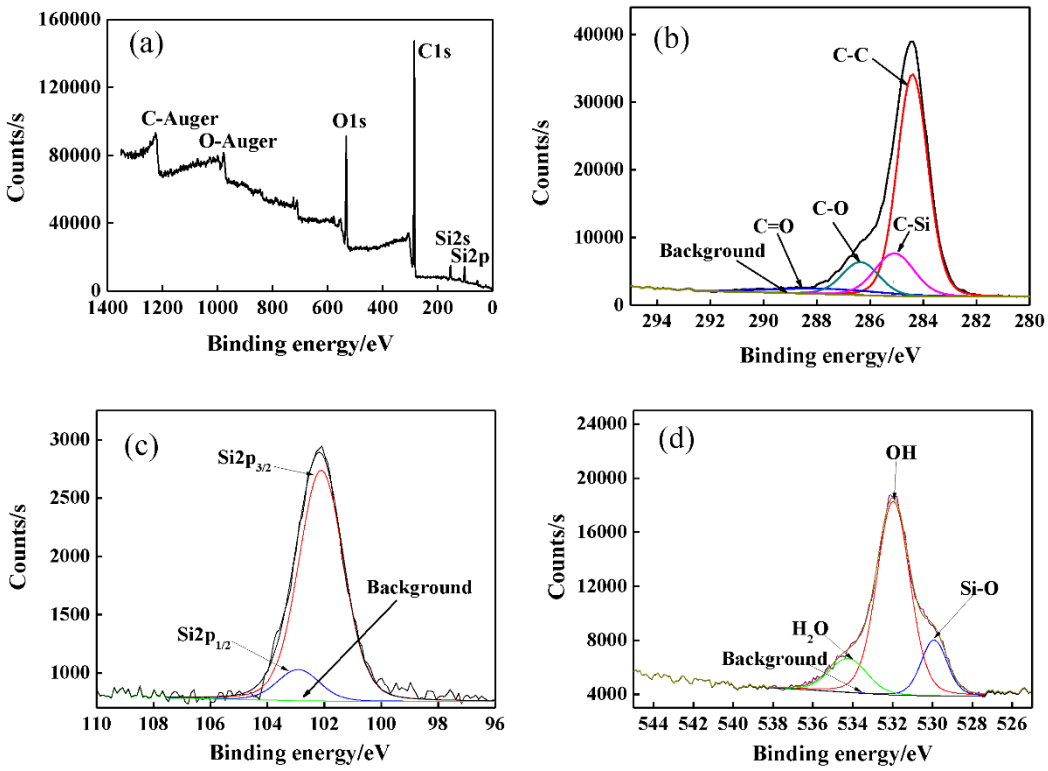

Fig. 5. (a) XPS full-san spectra of the hydrophobic HDTMS-TiO_2 coated mesh; (b)-(d) high resolution XPS spectra of C1s, Si2p, and O1s.

FT-IR spectra were characterized to determine the structures of the HDTMS-TiO_2 coated

mesh with the sintering temperature of 400 °C and the deposition time of 20 h, as shown in Fig. 6. The absorption peaks of 2880 cm^{-1}, 2925 cm^{-1} and 1460 cm^{-1} corresponded to the symmetric and the asymmetric stretching vibrations of $-CH_3$ and $-CH_2$ groups, respectively [57, 58], which indicated the presence of long chain alkyl hydrophobic mesh surface caused by HDTMS soles [53]. The peak at 1100 cm^{-1} attributed to the asymmetric stretching vibration of the Si-O species [57]. The wave numbers peaked at 862 cm^{-1} and 680 cm^{-1} indicated the presence of the groups of Ti-O-Si and Ti-O-Ti, respectively.[59] The peak of 800 cm^{-1} was the antisymmetric and symmetric stretching vibration of Si-C group [17]. The existence of these peaks proved the existence of the dehydration reaction between the hydrolytic HDTMS molecules and the TiO_2 nanoparticles, which confirmed the successful modification process.

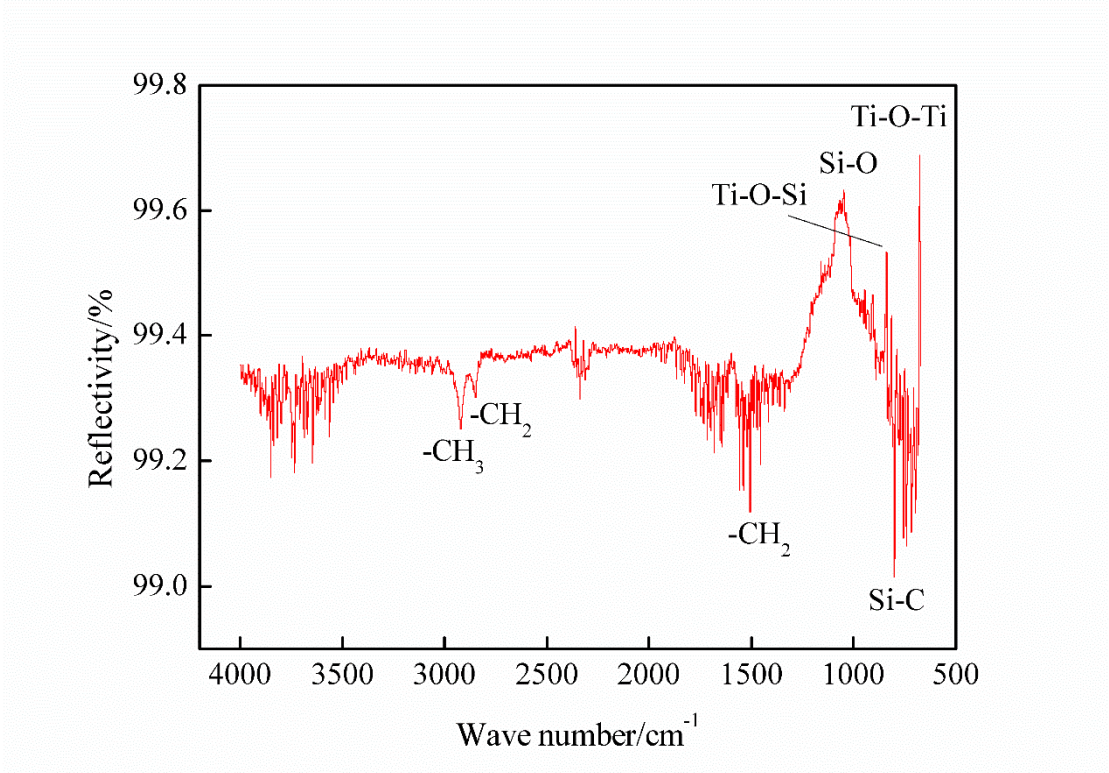

Fig. 6. FT-IR spectra of the as prepared HDTMS-TiO_2 coated mesh.

3.2. Surface wettability and oil penetration tests

Static contact angle. Fig. 7 shows the wetting behavior of the HDTMS-TiO_2 coated meshes prepared at three different deposition times of 5 h, 10 h, and 20 h at the same

sintering temperature of 400 °C. The corresponding contact angle were 125.5 ± 1.3°, 135.4 ± 0.4°, and 146.8 ± 2.2°, respectively, which indicated the hydrophobicity of the coated meshes. The results also indicated that the static water contact angle increased with increasing deposition time of the TiO_2 mesh in the mixture solution of $(NH_4)_2TiF_6$ and H_3BO_3. The reason is that the mesh surfaces become rougher with the increase of the TiO_2 particles deposited on the SS mesh, and the water contact angles consequently becomes larger under the same hydrophobic modification condition. All the water droplets were stable and could not penetrate the hydrophobic meshes due to the negative capillary effect [52, 60]. The visible non-sticky property of the hydrophobic mesh with water droplet contact angle of 146.8° is given in Supporting Information, Video S1.

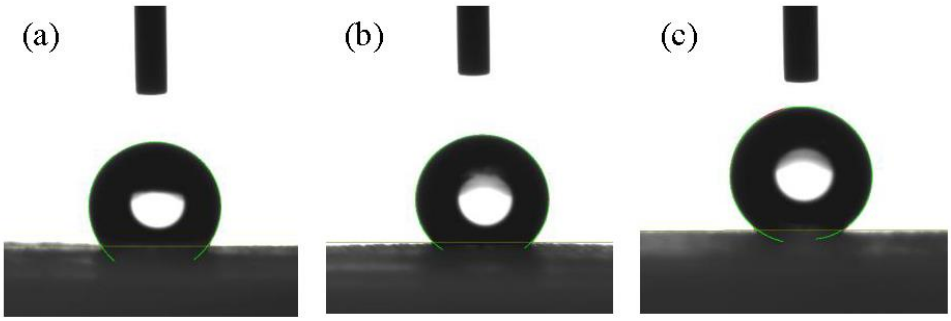

Fig. 7. Static contact angles of the HDTMS-TiO_2 coated meshes prepared at different deposition time. (a) 125.5 ± 1.3° at the deposition time of 5 h; (b) 135.4 ± 0.4° at 10 h; (c) 146.8 ± 2.2° at 20 h.

Self-cleaning and anti-fouling properties. The self-cleaning property of the hydrophobic HDTMS-TiO_2 coated mesh at the deposition time of 20 h and the sintering temperature of 400 °C was studied by immersing the mesh into the muddy water (clay content ~300 kg·m^{-3}), as shown in Fig. 8a-c and Supporting Information, Video S2. No muddy staying on the hydrophobic HDTMS-TiO_2 coated mesh when the mesh was immersed in the muddy water. The mesh was then lifted from the turbid solution and rinsed with DI water. The water was found still clean after washing the mesh.

To further estimate the self-cleaning property of the hydrophobic mesh, dusts of chalk powder were sprinkled on the mesh and then rinsed with a syringe filled with water. The

chalk powder was absorbed into the water flow as it rolled off the hydrophobic mesh surface, leaving a clean path on the mesh, as shown in Fig. 8d-f and Supporting Information, Video S3. These results proved that this hydrophobic mesh had excellent self-cleaning and anti-fouling properties. The self-cleaning property of the hydrophobic HDTMS-TiO_2 mesh may associate with the coaction of high capillary forces induced by water and the weak adhesion of the dusk particle to the hydrophobic surface.[61]

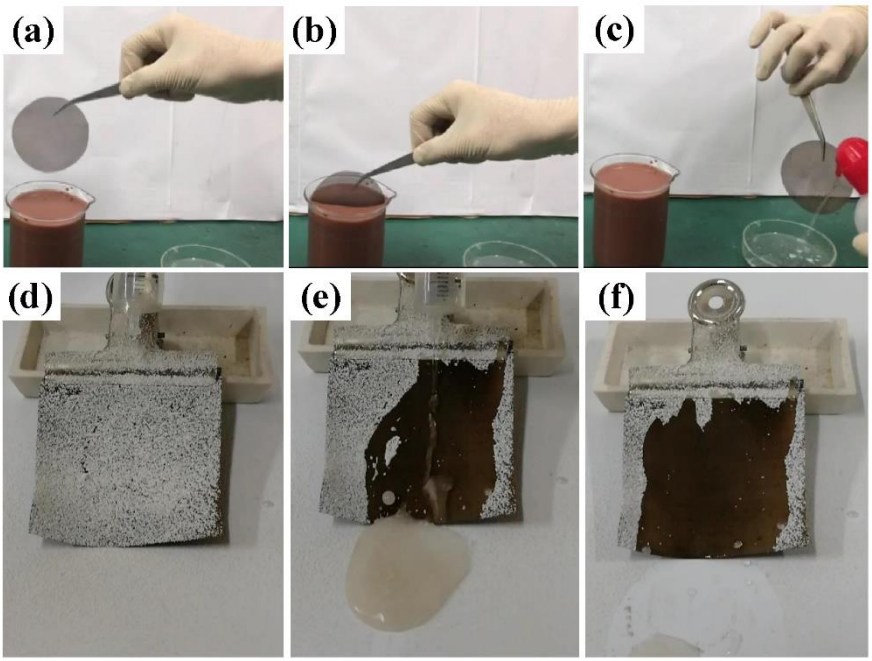

Fig. 8. Self-cleaning and antifouling tests of the HDTMS-TiO_2 coated mesh. (a) before mesh immersion in the muddy water; (b) immersing; (c) after immersion and rinse, indicating no muddy stayed on the mesh and self-cleaning property; (d) dusts of chalk power sprinkled on the hydrophobic mesh; (e) chalk powder absorbed into the water flow and (f) rolled off the mesh surface, leaving a clean path on the mesh.

Penetrating of the diesel oil. Fig. 9 demonstrates a screenshot of a diesel oil droplet spreading out over the hydrophobic HDTMS-TiO_2 mesh prepared at the sintering temperature of 400 °C and the deposition time of 20 h. The results indicated that the diesel oil droplet could expeditiously spread over the mesh surface and rapidly permeate through the mesh. This prepared hydrophobic mesh exhibited good spreading and fast

penetrating properties for the diesel oil and penetrated the hydrophobic mesh within 0.87 s which showed the super-oleophilic nature of the mesh (Supporting Information, Video S4). These marvelous behaviors of both non-sticking of water and permeating through oil made the hydrophobic meshes efficiently separate the oil/water mixture [14].

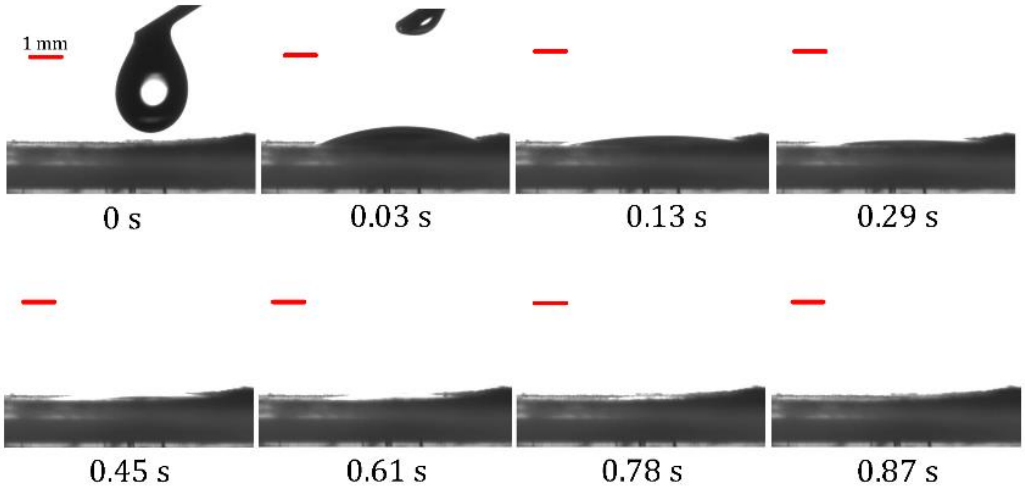

Fig. 9. Spreading and permeating behaviors of a diesel oil droplet on the hydrophobic HDTMS-TiO_2 coated mesh at the sintering temperature of 400 °C and the deposition time of 20 h. The scale bar is 1mm.

3.3. Intrusion pressure measurements and oil/water experiments

Fig. 10a shows the digital photography of the intrusion pressure testing of the hydrophobic HDTMS-TiO_2 coated meshes. Table 2 shows the intrusion pressure (ΔP_m *and* ΔP_c) and the separation efficiency (η), and the permeation flux (J) of the different hydrophobic HDTMS-TiO_2 coated meshes. For each experiment with the same coated mesh, at least three measurements were taken to get standard deviation. The maximum bearable height for the coated mesh at the sintering temperature of 400 °C and the deposition time of 20 h was about 17.5 ± 0.3 cm. Therefore, the maximum water intrusion pressure for the coated mesh was 1.7 ± 0.3 kPa. In other words, water could not penetrate the hydrophobic coated mesh under this pressure. The results also indicated that the intrusion pressure increased with the increase of the deposition time (Table 2). As a result, the intrusion pressure increased with the increase of the static contact angle (Fig. 7). The

intrusion pressure, however, was not significantly affected by the sintering temperature. Unfortunately, we have not found the relationship between the intrusion pressure and the efficiency of the oil-water separation. We inferred that the separation efficiency depended not only on the water contact angle (hydrophobicity) and the intrusion pressure, but also on the mesh size and the property of the water-oil mixtures (viscosity, oil type, and surfactant, etc.). Actually, in our previous work [14], we found that although this mesh reached the super-hydrophobicity and high intrusion pressure, the as-prepared Ni-P mesh almost lost their separation performance because the mesh was blocked with the Ni-P particles and the mesh size was very small. As a result, further research would be necessary to uncover the relationship among the separation efficiency, the intrusion pressure, the wettability, as well as the pore size of the separating mesh.

As mentioned above, the hydrophobic HDTMS-TiO_2 coated meshes had priority in penetrating the oil, whereas the water droplet was not wetted and could not penetrate the meshes holes. These results made the hydrophobic HDTMS-TiO_2 coated meshes the very promising materials for oil/water separation. The video screenshot of the typical oil/water mixtures separation process under solely gravity-driven is shown in Fig. 10b. Table 2 indicates that almost all of the separation efficiency, η, of the hydrophobic coated meshes are larger than 98.0% for the mixture of diesel oil and water. By comparison, these results could be compared with those in the published literatures. For example, Li et al. [62] fabricated a superhydrophobic attapulgite coated mesh with a water contact angle of 155±1° separation efficiency up to 97% for the kerosene/water mixture. Liu et al. [63] obtained superhydrophobic stainless steel mesh treated with $CuCl_2$ and HCl solution and subsequently modified with stearic acid. The as-prepared mesh had a water contact angle of 153±3°, and the separation efficiency was more than 93%. Shi et al. [64] prepared the superhydrophobic and superoleophilic copper mesh via thermal oxidation and subsequently surface modified with dodecanthiol-ethanol solution. The water contact angle of the as-prepared mesh was up to 162° and the separation efficiency of above 95% for oil-water mixture. Compared to the reported data, we could see that the separation efficiency of the as-prepared hydrophobic HDTMS-TiO_2 meshes for oil/water mixtures

were equivalent or higher than those of the previously obtained superhydrophobic coated meshes.

In addition to the separation efficiency, the permeate flux is another crucial property applicated in evaluating the oil/water separation effect because higher permeate flux in a mesh leads to faster separation in the industry. [21] Thus, the permeate flux of the hydrophobic HDTMS-TiO_2 coated meshes were also measured during the oil/water separation tests. The permeate flux was obtained by placing the beaker of the oil outlet on the electronic balance and metering the oil weight for 30 s at the stable stage of each oil-water separation test. We found that the oil/water mixture was filled with the entire mesh section area during the stable stage of the separation experiment, as shown in Fig. 10b and Supporting Information, Video S5. Therefore, the effective area of *S* in Eq. (3) could be calculated according to the inside diameter of the organic glass tubes. Table 2 shows the permeation flux, *J*, with different coated meshes. The results indicated that the highest permeate flux occurred at the minimum deposition time of the TiO_2 coating. Furthermore, the separation efficiency increased slightly with the increase of the deposition time, while the permeate flux decreased as the deposition time increasing (Table 2). The different separation efficiency and the permeate flux of the five meshes might be ascribed to their different mesh sizes because of the different thickness of the TiO_2 coating layers with different deposition time [40]. Furthermore, the permeate fluxes of the as-prepared hydrophobic HDTMS-TiO_2 coating meshes were comparable with the published results obtained from the superhydrophobic coating meshes [65-67].

The oil-water separating mechanism of the hydrophobic HDTMS-TiO_2 meshes could be theoretically elucidated according to the intrusion pressure (ΔP_c):[54]

$$\Delta P_c = \frac{2\gamma_{wo}}{R} = -\frac{2C\gamma_{wo}\cos\theta_w}{A} \quad (4)$$

where γ_{wo} is the interfacial tension between water and oil; *R* is the radius of the meniscus; θ_w represents the water contact angle on the mesh; *C* and *A* denote the circumference and the cross-sectional area of the mesh pore, respectively. According to Eq. (4), the intrusion pressure (ΔP_c) of the mesh for water was positive (negative capillary effect [54] in the oil-water-air three phase interface) because the water contact angle was $\theta_w > 90°$

(hydrophobicity, see Fig. 7) on the HDTMS-TiO_2 mesh surface. Therefore, the water could not spontaneously permeate the hydrophobic mesh. As a result, the mesh could withstand some extent of water pressure (Fig. 10a). On the other hand, the mesh could not support any oil pressure, and led to the oil spontaneously permeating because the ΔP_c of the mesh for oil was negative (capillary effect [54]) and the oil contact angle was $\theta_o < 90°$ (lipophilicity, see Fig. 9) on the hydrophobic HDTMS-TiO_2 mesh. More important, Eq. (4) indicated that the obtained separation mechanism of oil and water was mainly based on the incompatible wetting property of oil (lipophilicity) and water (hydrophobicity) on the separating mesh. According to the theoretical analysis and the experimental results, we confirmed that the as-prepared hydrophobic coating meshes ($\theta_w > 90°$) could obtain equivalent or higher separation properties compared with the previously reported superhydrophobic coated meshes. In other words, the superhydrophobicity ($\theta_w > 150°$) of the separating mesh was nonessential for the highly efficient oil-water separation.

The intrusion pressure (ΔP_c) of the hydrophobic coating mesh could be evaluated with Eq. (4) based on the data of the pore size from Fig. 4b, the θ_w data from Fig. 7, the interfacial tension, γ_{wo}, between water and diesel oil[68], as well as the coating thickness provided in the literature[40]. Table 2 indicates that the ΔP_c value was larger than the ΔP_m. The reason might be that the measured value of the pore size of the coating mesh was less using SEM and the sample size of the hole was relatively small. The relative error for the coating mesh of the depositing time of 20 h, 10 h, and 5 h was 11.7%, 25.0%, and 18.1%, respectively.

Fig. 10. Digital photography of (a) the intrusion pressure testing and (b) the video screenshot of the typical oil/water mixtures separation process of the hydrophobic HDTMS-TiO_2 coated meshes.

Table 2. The intrusion pressure (ΔP_m and ΔP_c) and the separation efficiency (η), and the permeation flux (J) of the different hydrophobic HDTMS-TiO_2 coated meshes.

Deposition time/h	Sintering temperature/°C	ΔP_m/kPa	ΔP_c/kPa	η/%	J/mL·m^{-2}·s^{-1}
5	400	1.1 ± 0.4	1.3 ± 0. 4	97.6 ± 0.7	504.3 ± 19.6
10	400	1.2 ± 0.2	1.6 ± 0. 1	98.2 ± 1.4	479.9 ± 12.7
10	300	1.2 ± 0.5	-	98.1 ± 0.6	449.4 ± 9.3
10	500	1.3 ± 0.2	-	98.2 ± 0.8	490.1 ± 15.4
20	400	1.7 ± 0.3	1.9 ± 0. 2	98.8 ± 1.3	463.7 ± 18.3

Note: ΔP_m - the measured intrusion pressure; ΔP_c - the calculated intrusion pressure.

3.4 Reusability of the meshes

In oil/water separation field, the key issue for the actual application is the reusability of the meshes.[69] Herein, the oil/water separation efficiency versus the recycle numbers was also investigated by taking the diesel oil/water mixture as an example. To recover the hydrophobicity of the mesh after each oil/water separation experiment, the mesh was rinsed with sufficient alcohol and distilled water to remove the oil on the surface, and then it was dried under atmospheric conditions. Fig. 11a showed that the hydrophobic coated mesh kept the separation efficiency above 97.8% after 35 separation cycles. Fig. 11b shows that the water contact angle of the hydrophobic mesh decreased considerably from 146.8 ± 2.2° to 140.3 ± 4.5° within 5 separation cycles which coincided exactly with that of Wang et al. [17]. The result suggested that some HDTMS compound might be gradually dissolved in the oil phase and washed away during the cleaning process after each oil/water separation. However, the water contact angle was not changed significantly from 6 to 35 separation cycles which indicated that the oil could not severely damage the hydrophilicity of the mesh. More important, the mesh still retained hydrophobic state

after 35 separation cycles. These results exhibited a good stability of the hydrophobic HDTMS-TiO_2 coated mesh.

The separation efficiency for a range of oil/water mixtures was also determined, as shown in Fig. 11c. The calculated separation efficiencies of the hydrophobic HDTMS-TiO_2 coated meshes for various oils were above 98.0% and the oil types had virtually no effect on the separation efficiencies, indicating that these hydrophobic meshes had general suitability for various oil/water mixtures separation.

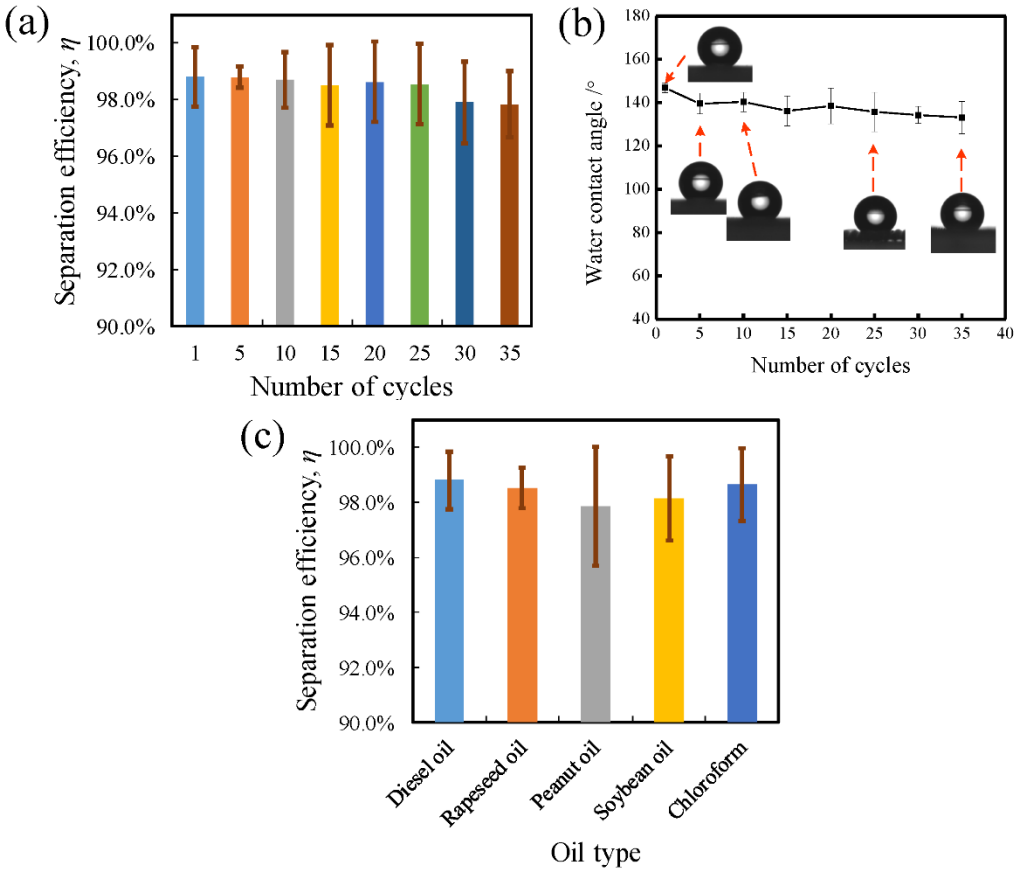

Fig. 11. (a) The recycle numbers of oil/water separation by taking the diesel oil/water mixture as an example; (b) water contact angles of the different recycle numbers on the hydrophobic HDTMS-TiO_2 coated mesh; (c) the separation efficiency of the hydrophobic HDTMS-TiO_2 coated mesh for various oil/water mixtures. The insets in Fig. 11b show the corresponding water contact angle images.

4. Conclusions

The fluorine-free hydrophobic HDTMS-TiO_2 coated meshes were prepared by the liquid phase deposition method and the subsequent hydrophobic treatment. The largest static contact angle and the maximum water intrusion pressure of the HDTMS-TiO_2 coated mesh was 146.8 ± 2.2° and 1.7 ± 0.3 kPa, respectively. The as-prepared hydrophobic meshes exhibited a favorable self-cleaning property and were general suitable for various oil/water separations. The obtained hydrophobic coating mesh held the separation efficiency of higher than 98.0% for many types of the oil/water mixtures and kept above 97.8% after 35 separating cycles, indicating their highly efficient oil-water separation and good stability for long time usage. The theoretical analysis and the experimental results both indicated that the superhydrophobicity of the separating mesh was nonessential for the highly efficient oil-water separation. This finding might provide a new perspective on application of the coating meshes with special wetting properties in oil/water separation field. In short, due to the prominent oil/water separation property, the fluorine-free hydrophobic HDTMS-TiO_2 coated meshes would be a beneficial option to the potential practical values for economically separating the industrial oily wastewater mixtures and the environmental oil spills.

Supplementary data

Supplementary materials, Video S1 to S5, to this article can be found in the online version.

Notes

The authors declare no competing financial interest.

Acknowledgements

This study was funded by General Project of Chongqing Foundation and Frontier Research Project, China (Grant No. KJ1400912), Scientific and Technological Research Program of Chongqing Municipal Education Commission, China (Grant No. cstc2014jcyjA90009).

Conflict of interest

The authors declare no competing financial interest.

Corresponding authors

*Yongwei Cai. Tel.: +86 23 6256 3617. Fax: +86 23 6256 3221. E-mail address: cyw@cqut.edu.cn (Y. Cai).

*Qi Zhao. Tel.: +44 1382 385651; Fax: +44 1382 385508. E-mail address: q.zhao@dundee.ac.uk (Q. Zhao).

References

[1] L. Yu, M. Han, F. He, A review of treating oily wastewater, Arab. J. Chem. 10 (2017) S1913-S1922.

[2] T.J. Crone, M. Tolstoy, Magnitude of the 2010 Gulf of Mexico oil leak, Science 330 (2010) 634.

[3] X. Li, M. Cao, H. Shan, F.H. Tezel, B. Li, Facile and scalable fabrication of superhydrophobic and superoleophilic PDMS-co-PMHS coating on porous substrates for highly effective oil/water separation, Chem. Eng. J. 358 (2019) 1101-1113.

[4] X. Gao, G. Wen, Z. Guo, Durable superhydrophobic and underwater superoleophobic cotton fabrics growing zinc oxide nanoarrays for application in separation of heavy/light oil and water mixtures as need, Colloids Surf. A 559 (2018) 115-126.

[5] P. Kundu, I.M. Mishra, Treatment and reclamation of hydrocarbon-bearing oily wastewater as a hazardous pollutant by different processes and technologies: A state-of-the-art review, Rev. Chem. Eng. 35 (2018) 73-108.

[6] M. Hu, H. Niu, X. Chen, H. Zhan, Natural cellulose microfiltration membranes for oil/water nanoemulsions separation, Colloids Surf. A 564 (2019) 142-151.

[7] A.B. Nordvik, J.L. Simmons, K.R. Bitting, A. Lewis, T. Strøm-Kristiansen, Oil and water separation in marine oil spill clean-up operations, Spill Sci. Technol. B. 3 (1996) 107-122.

[8] J. Song, Y. Lu, J. Luo, S. Huang, L. Wang, W. Xu, I.P. Parkin, Barrel-shaped oil skimmer designed for collection of oil from spills, Adv. Mate. Interfaces 2 (2015) 1500350-1500357.

[9] D. Wu, L. Fang, Y. Qin, W. Wu, C. Mao, H. Zhu, Oil sorbents with high sorption capacity, oil/water selectivity and reusability for oil spill cleanup, Mar. Pollut. Bull. 84 (2014) 263-267.

[10] G.B. Demirel, E. Aygül, Robust and flexible superhydrophobic/superoleophilic melamine sponges for oil-water separation, Colloids Surf. A 577 (2019) 613-621.

[11] A.A. Al-Shamrani, A. James, H. Xiao, Destabilisation of oil-water emulsions and separation by dissolved air flotation, Water Res. 36 (2002) 1503-1512.

[12] M. Liu, S. Wang, L. Jiang, Nature-inspired superwettability systems, Nat. Rev. Mater. 2 (2017) 17036.

[13] D. Zhang, L. Li, Y. Wu, W. Sun, J. Wang, H. Sun, One-step method for fabrication of superhydrophobic and superoleophilic surface for water-oil separation, Colloids Surf. A 552 (2018) 32-38.

[14] Y. Cai, S. Li, Z. Cheng, G. Xu, X. Quan, Y. Zhou, Facile fabrication of super-hydrophobic FAS modified electroless Ni-P coating meshes for rapid water-oil separation, Colloids Surf. A 540 (2018) 224-232.

[15] J. Li, D. Li, Y. Yang, J. Li, F. Zha, Z. Lei, A prewetting induced underwater superoleophobic or underoil (super) hydrophobic waste potato residue-coated mesh for selective efficient oil/water separation, Green Chem. 18 (2016) 541-549.

[16] Z. Chu, Y. Feng, S. Seeger, Oil/water separation with selective superantiwetting/superwetting surface materials, Angew. Chem. Int. Edit. 54 (2015) 2328-2338.
[17] Q. Wang, M. Yu, G. Chen, Q. Chen, J. Tian, Robust fabrication of fluorine-free superhydrophobic steel mesh for efficient oil/water separation, J. Mater. Sci. 52 (2017) 2549-2559.
[18] M. Khosravi, S. Azizian, Preparation of superhydrophobic and superoleophilic nanostructured layer on steel mesh for oil-water separation, Sep. Purif. Technol. 172 (2017) 366-373.
[19] C. Zhou, J. Feng, J. Cheng, H. Zhang, J. Lin, X. Zeng, P. Pi, Opposite superwetting nickel meshes for on-demand and continuous oil/water separation, Ind. Eng. Chem. Res. 57 (2018) 1059-1070.
[20] L. Feng, Z. Zhang, Z. Mai, Y. Ma, B. Liu, L. Jiang, D. Zhu, A super-hydrophobic and super-oleophilic coating mesh film for the separation of oil and water, Angew. Chem. Int. Edit. 116 (2004) 2046-2048.
[21] C. Yang, Y. Wang, H. Fu, S. Yang, Y. Zhu, H. Yue, W. Jiang, B. Liang, A stable eco-friendly superhydrophobic/superoleophilic copper mesh fabricated by one-step immersion for efficient oil/water separation, Surf. Coat. Technol. 359 (2019) 108-116.
[22] Z. Xu, D. Jiang, Z. Wei, J. Chen, J. Jing, Fabrication of superhydrophobic nano-aluminum films on stainless steel meshes by electrophoretic deposition for oil-water separation, Appl. Surf. Sci. 427 (2018) 253-261.
[23] Z. Dong, B. Wang, M. Liu, X.H. Ma, Z.L. Xu, A self-cleaning TiO_2 coated mesh with robust underwater superoleophobicity for oil/water separation in a complex environment, RSC Adv. 6 (2016) 65171-65178.
[24] S. Giessler, E. Just, R. Störger, Easy-to-clean properties-Just a temporary appearance? Thin Solid Films 502 (2006) 252-256.
[25] N. Cohen, A. Dotan, H. Dodiuk, S. Kenig, Superhydrophobic coatings and their durability, Mater. Manuf. Process. 31 (2016) 1143-1155.
[26] K.S. Kumar, V. Kumar, C.R. Nair, Bulk superhydrophobic materials: a facile and efficient approach to access superhydrophobicity by silane and urethane chemistries, J. Mater. Chem. A 2 (2014) 15502-15508.
[27] L. Chen, Z. Guo, A facile method to mussel-inspired superhydrophobic thiol-textiles@ polydopamine for oil/water separation, Colloids Surf. A 554 (2018) 253-260.
[28] W. Zhou, G. Li, L. Wang, Z. Chen, Y. Lin, A facile method for the fabrication of a superhydrophobic polydopamine-coated copper foam for oil/water separation, Appl. Surf. Sci. 413 (2017) 140-148.
[29] J.I. Tapia, E. Alvarado-Gómez, A. Encinas, Non-expensive hydrophobic and magnetic melamine sponges for the removal of hydrocarbons and oils from water, Sep. Purif. Technol. 222 (2019) 221-229.
[30] Y. Cai, M. Liu, L. Hui, $CaCO_3$ fouling on microscale-nanoscale hydrophobic titania-fluoroalkylsilane films in pool boiling, AIChE J. 59 (2013) 2662-2678.
[31] Y.Y. Yan, N. Gao, W. Barthlott, Mimicking natural superhydrophobic surfaces and grasping the wetting process: A review on recent progress in preparing superhydrophobic surfaces, Adv. Colloid Interfac. 169 (2011) 80-105.
[32] T. Nishino, M. Meguro, K. Nakamae, M. Matsushita, Y. Ueda, The lowest surface free energy based on -CF_3 alignment, Langmuir 15 (1999) 4321-4323.
[33] C. Anitha, S. Mayavan, Salvinia inspired fluroine free superhydrophobic coatings, Appl. Surf.

Sci. 449 (2018) 250-260.
[34] D.A. Ellis, S.A. Mabury, J.W. Martin, D.C.G. Muir, Thermolysis of fluoropolymers as a potential source of halogenated organic acids in the environment, Nature 412 (2001) 321.
[35] C. Schlaich, L. Yu, L.C. Camacho, Q. Wei, R. Haag, Fluorine-free superwetting systems: construction of environmentally friendly superhydrophilic, superhydrophobic, and slippery surfaces on various substrates, Polym. Chem-UK 7 (2016) 7446-7454.
[36] S. Gao, X. Dong, J. Huang, S. Li, Y. Li, Z. Chen, Y. Lai, Rational construction of highly transparent superhydrophobic coatings based on a non-particle, fluorine-free and water-rich system for versatile oil-water separation, Chem. Eng. J. 333 (2018) 621-629.
[37] H. Wang, S. Dong, Z. Wang, One-step fabrication of superhydrophobic surface on beryllium copper alloys and corrosion protection application, Colloids Surf. A 556 (2018) 291-298.
[38] D. Nanda, A. Sahoo, A. Kumar, B. Bhushan, Facile approach to develop durable and reusable superhydrophobic/superoleophilic coatings for steel mesh surfaces, J. Colloid. Interf. Sci. 535 (2019) 50-57.
[39] J. Huser, S. Bistac, M. Brogly, C. Delaite, T. Lasuye, B. Stasik, Investigation on the adsorption of alkoxysilanes on stainless steel, Appl. Spectrosc. 67 (2013) 1308-1314.
[40] Y. Cai, M. Liu, Corrosion behavior of titania films coated by liquid-phase deposition on AISI304 stainless steel substrates, AIChE J. 58 (2012) 1907-1920.
[41] S. Jo, Y. Kim, Superhydrophilic–underwater superoleophobic TiO_2-coated mesh for separation of oil from oily seawater/wastewater, Korean J. Chem. Eng. 33 (2016) 3203-3206.
[42] M. Shaker, E. Salahinejad, F. Ashtari-Mahini, Hydrophobization of metallic surfaces by means of Al_2O_3-HDTMS coatings, Appl. Surf. Sci. 428 (2018) 455-462.
[43] K. Tadanaga, N. Katata, T. Minami, Formation process of super-water-repellent Al_2O_3 coating films with high transparency by the Sol-Gel method, J. Am. Ceram. Soc. 80 (1997) 3213-3216.
[44] J. Li, D. Li, W. Li, H. Li, H. She, F. Zha, Facile fabrication of underwater superoleophobic SiO_2 coated meshes for separation of polluted oils from corrosive and hot water, Sep. Purif. Technol. 168 (2016) 209-214.
[45] J. Li, R. Kang, X. Tang, H. She, Y. Yang, F. Zha, Superhydrophobic meshes that can repel hot water and strong corrosive liquids used for efficient gravity-driven oil/water separation, Nanoscale 8 (2016) 7638-7645.
[46] N. Lorwanishpaisarn, P. Kasemsiri, N. Srikhao, K. Jetsrisuparb, J.T.N. Knijnenburg, S. Hiziroglu, U. Pongsa, P. Chindaprasirt, Fabrication of durable superhydrophobic epoxy/cashew nut shell liquid based coating containing flower-like zinc oxide for continuous oil/water separation, Surf. Coat. Technol. 366 (2019) 106-113.
[47] A.K. Singh, J.K. Singh, Fabrication of zirconia based durable superhydrophobic-superoleophilic fabrics using non fluorinated materials for oil–water separation and water purification, RSC Adv. 6 (2016) 103632-103640.
[48] R. Liu, S. Young, S. Dangwal, I. Shaik, E. Echeverria, D. McIlroy, C. Aichele, S. Kim, Boron substituted MFI-type zeolite-coated mesh for oil-water separation, Colloids Surf. A 550 (2018) 108-114.
[49] L. Ćurković, H.O. Ćurković, S. Salopek, M.M. Renjo, S. Šegota, Enhancement of corrosion protection of AISI 304 stainless steel by nanostructured sol-gel TiO_2 films, Corros. Sci. 77 (2013) 176-184.
[50] M.A. Gondal, M.S. Sadullah, M.A. Dastageer, G.H. McKinley, D. Panchanathan, K.K. Varanasi,

Study of factors governing oil-water separation process using TiO_2 films prepared by spray deposition of nanoparticle dispersions, ACS App. Mater. Inter. 6 (2014) 13422-13429.

[51] S. Deki, Y. Aoi, O. Hiroi, A. Kajinami, Titanium (IV) oxide thin films prepared from aqueous solution, Chem. Lett. 25 (1996) 433-434.

[52] C. Yeom, Y. Kim, Purification of oily seawater/wastewater using superhydrophobic nano-silica coated mesh and sponge, J. Ind. Eng. Chem. 40 (2016) 47-53.

[53] L. Xu, L. Wang, Y. Shen, Y. Ding, Z. Cai, Preparation of hexadecyltrimethoxysilane-modified silica nanocomposite hydrosol and superhydrophobic cotton coating, Fiber Polym. 16 (2015) 1082-1091.

[54] J. Li, R. Kang, Y. Zhang, M. Li, H. She, F. Zha, Z. Lei, Facile fabrication of superhydrophobic meshes with different water adhesion and their influence on oil/water separation, RSC Adv. 6 (2016) 90824-90830.

[55] B.V. Crist, Handbooks of monochromatic XPS spectra: Volume 1 The elements of native oxides, XPS International L.L.C., 1999.

[56] N. Graf, E. Yegen, T. Gross, A. Lippitz, W. Weigel, S. Krakert, A. Terfort, W. E. S. Unger, XPS and NEXAFS studies of aliphatic and aromatic amine species on functionalized surfaces, Surf. Sci. 603 (2009) 2849-2860.

[57] C. Li, Y. Sun, M. Cheng, S. Sun, S. Hu, Fabrication and characterization of a TiO_2/polysiloxane resin composite coating with full-thickness super-hydrophobicity, Chem. Eng. J. 333 (2018) 361-369.

[58] Z. Yang, X. Liu, Y. Tian, Fabrication of super-hydrophobic nickel film on copper substrate with improved corrosion inhibition by electrodeposition process, Colloids Surf. A 560 (2019) 205-212.

[59] U.S. Handajani, A.A. Widati, I.N. Yusbainika, Preparation hydrophobic fabric coated by TiO_2 and hexadecyltrimethoxysilane, IOP Publishing 2019.

[60] X. Li X, B.K. Tay, P. Miele, A. Brioude, D. Cornu, Fabrication of silicon pyramid/nanowire binary structure with superhydrophobicity, Appl. Surf. Sci. 255 (2009) 7147-7152.

[61] F. Su, K. Yao, Facile fabrication of superhydrophobic surface with excellent mechanical abrasion and corrosion resistance on copper substrate by a novel method, ACS Appl. Mater. Interfaces 6 (2014) 8762-8770.

[62] J. Li, L. Yan, H. Li, J. Li, F. Zha, Z. Lei, A facile one-step spray-coating process for the fabrication of a superhydrophobic attapulgite coated mesh for use in oil/water separation, RSC Adv. 5 (2015) 53802-53808.

[63] Y. Liu, K. Zhang, W. Yao, J. Liu, Z. Han, L. Ren, Bioinspired structured superhydrophobic and superoleophilic stainless steel mesh for efficient oil-water separation, Colloids Surf. A 500 (2016) 54-63.

[64] Y. Shi, W. Yang, X. Feng, Y. Wang, G. Yue, S. Jin, Fabrication of superhydrophobic-superoleophilic copper mesh via thermal oxidation and its application in oil–water separation, Appl. Surf Sci. 367 (2016) 493-499.

[65] E. Velayi, R. Norouzbeigi, Synthesis of hierarchical superhydrophobic zinc oxide nano-structures for oil/water separation, Ceram. Int. 44 (2018) 14202-14208.

[66] H. Cao, J. Fu, Y. Liu, Y. Liu, S. Chen, Facile design of superhydrophobic and superoleophilic copper mesh assisted by candle soot for oil water separation[J]. Colloids Surf. A 537 (2018) 294-302.

[67] H. Cao, W. Gu, J. Fu, Y. Liu, S. Chen, Preparation of superhydrophobic/oleophilic copper mesh for oil-water separation, Appl. Surf. Sci. 412 (2017) 599-605.
[68] M. Bettahar, G. SchÄfer, M. Baviere, An optimized surfactant formulation for the remediation of diesel oil polluted sandy aquifers, Environ. Sci. Technol. 33 (1999) 1269-1273.
[69] X.J. Zeng, S.P. Xu, P.H. Pi, J. Cheng, L. Wang, S.F. Wang, X.F. Wen, Polymer-infiltrated approach to produce robust and easy repairable superhydrophobic mesh for high-efficiency oil/water separation, J. Mater. Sci. 53 (2018) 10554-10568.

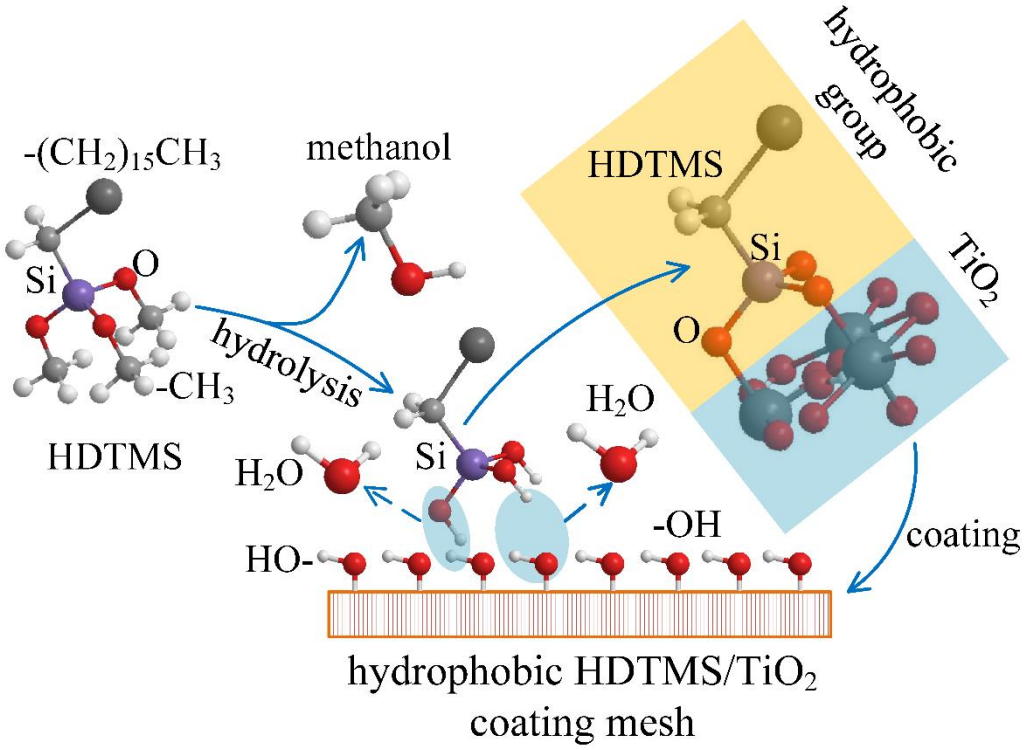

Graphical abstract